BBA - Molecular Cell Research 1870 (2023) 119429

Contents lists available at ScienceDirect

BBA - Molecular Cell Research

journal homepage: www.elsevier.com/locate/bbamcr

Research paper

Mitochondrial dysfunction mediates neuronal cell response to DMMB photodynamic therapy

Raphael de Ávila Narciso Gomes [a,b,1], Alejandro Marmolejo-Garza [a,c,1], Floris-Jan Haan [a], Teresa Mitchell García [a], Tingting Chen [a], Mario Mauthe [d], Yollanda E. Moreira Franco Parisotto [e], Mario Minor Murakami Jr [e], Suely Kazue Nagahashi Marie [e], Maurício S. Baptista [b], Amalia M. Dolga [a,*], Marina Trombetta-Lima [a,c,*]

[a] Faculty of Science and Engineering, Department of Molecular Pharmacology, Groningen Research Institute of Pharmacy (GRIP), University of Groningen, 9713 AV Groningen, the Netherlands
[b] Chemistry Institute, Biochemistry Department, University of São Paulo (USP), 05508-000 São Paulo, Brazil
[c] Department of Biomedical Sciences of Cells and Systems, Section Molecular Neurobiology, University of Groningen, University Medical Center Groningen, 9713 AV Groningen, the Netherlands
[d] Department of Biomedical Sciences of Cells and Systems, Section Molecular Cell Biology, University of Groningen, University Medical Center Groningen, 9713 AV Groningen, the Netherlands
[e] Medical School, Neurology Department, University of São Paulo (USP), 01246903 São Paulo, Brazil

ARTICLE INFO

Keywords:
Photodynamic therapy
1,9-Dimethyl-methylene blue
Mitochondrial dysfunction
Phenothiazines
Central nervous system
Phototoxicity

ABSTRACT

Photodynamic therapy (PDT) is a process in which a photosensitizer (PS) is exposed to specific wavelengths and generates reactive oxygen species (ROS) which act within nanometers. The low invasive nature and directed cytotoxicity of this approach render it attractive to the treatment of different conditions, including the ones that affect the central nervous system (CNS). The effect of PDT on healthy neurons is one main concern over its use in the CNS, since neuronal-like cells were shown to be particularly sensitive to certain PSs. Among available PSs, 1,9-dimethyl-methylene blue (DMMB) stands out as being resistant to reduction to its inactive leuco form and by being able to produce high levels of singlet-oxygen. In this study, we aimed to investigate DMMB photodamage mechanisms in the hippocampal cell line HT22. Our results demonstrate that DMMB-PDT decrease in cell viability was linked with an increase in cell death and overall ROS production. Besides, it resulted in a significant increase in mitochondrial ROS production and decreased mitochondria membrane potential. Furthermore, DMMB-PDT significantly increased the presence of acidic autolysosomes, which was accompanied by an increase in *ATG1* and *ATG8* homologue *GaBarap1* expression, and decreased *DRAM1* expression. Taken together our results indicated that mitochondrial and autophagic dysfunction underlie DMMB-PDT cytotoxicity in neuronal cells.

1. Introduction

Photodynamic therapy (PDT) is a promising approach for cancer therapy in which a photosensitizer (PS) is exposed to specific wavelengths to generate reactive oxygen species (ROS) [1,2]. The resulting oxidant species damage biomolecules within nanometers range of the PS, making it possible to target specific subcellular compartments, depending on its affinity [3,4]. The low invasive nature and directed

Abbreviations: ATP, adenosine triphosphate; PDT, photodynamic therapy; PS, photosensitizer; ROS, reactive oxygen species; MB, methylene blue; PBS, phosphate-buffered saline; DMMB, 1,9-Dimethyl-Methylene Blue; PI, propidium iodide; DMSO, dimethyl sulfoxide; MTT, 3-(4,5-dimethyl-2-thiazolyl)-2,5-diphenyl-2H-tetrazolium bromide; PFA, paraformaldehyde; CNS, central nervous system; LC3, microtubule-associated protein 1 (MAP1) light chain 3.

* Corresponding authors at: Faculty of Science and Engineering, Groningen Research Institute of Pharmacy, Department of Molecular Pharmacology, University of Groningen, Antonius Deusinglaan 1, Groningen, the Netherlands.
E-mail addresses: a.m.dolga@rug.nl (A.M. Dolga), m.trombetta.lima@rug.nl (M. Trombetta-Lima).
[1] Both authors contributed equally to this work.

https://doi.org/10.1016/j.bbamcr.2022.119429
Received 10 March 2022; Received in revised form 20 December 2022; Accepted 29 December 2022
Available online 3 January 2023

cytotoxicity of the system renders it attractive to the treatment of different conditions, ranging from macular degeneration to infections and tumors [5–7]. In the central nervous system (CNS), despite its challenging access routes, PDT has been applied to tumor treatment and fluorescence-guided surgical resection with beneficial results [8,9]. Nonetheless, attention must be given to PDT potential off-target effects on neurons, which have been shown to be sensitive and prone to cell death by different activated PS, such as porfimer sodium, Deuteroporphyrin IX and Hematoporphyrin derivatives, while being less sensitive to others, such as meta-tetrahydroxyphenyl chlorin [7,10–12].

Among the available PSs, the phenothiazinium chromophore methylene blue (MB) stands out by efficiently reaching the CNS by crossing the blood brain barrier [13,14]. In fact, without light activation, MB has neuroprotective properties. The MB phenothiazinium salt acts as an electron carrier that bypasses complex I/III blockage, transferring electrons from NADH to reduce cytochrome *c*. As a result, electron leakage and ROS production decrease while adenosine triphosphate (ATP) increases [15]. Moreover, MB was reported to reverse the Warburg effect and inhibit proliferation in glioblastoma cells by increasing O_2 consumption and reducing lactate formation [16]. However, high doses are required for MB activity, leading to off target effects [17]. Following red light activation, MB is an efficient cytotoxic agent in vitro, acting through the increase of overall ROS production [4,18].

Interestingly, as an illustration of MB potential on neurodegenerative diseases, activated MB has been shown to induce the dissociation of $A\beta_{42}$ aggregates through their oxidation in a Drosophila model [19]. Taken together, these data illustrate the potential of MB mediated-PDT for neuropathology treatment and foster the search of MB derivatives with optimized activity for various clinical applications.

Among them, MB's methylated derivative 1,9-dimethyl-methylene blue (DMMB) stands out as more resistant to reduction to its inactive leuco form, and by being able to produce higher levels of singlet-oxygen when compared to MB [4,20]. Nevertheless, our group recently showed that DMMB, but not MB, induces mitochondrial damage and impaired mitophagy in keratinocytes [4]. DMMB's higher phototoxicity might suggest that DMMB could be a more efficient PS when compared to MB, especially when considering its use in the CNS, since neurons are heavily dependent on mitochondrial metabolism [21].

In light of the potential DMMB applicability for neurodegenerative diseases and CNS tumors, here we investigated DMMB-PDT photodamage mechanisms in the hippocampal cell line HT22 to better assess its applicability to the CNS.

2. Materials and methods

2.1. Cell culture

Primary cortical neurons were prepared from embryonic (E13–14) C57BL/6 mice (mixed gender) under sterile conditions. The cortices from embryos were collected and treated with 0.2 mg/mL trypsin at 37 °C for 15 min. After DNase and trypsin inhibitor treatment, the cell pellet was obtained through centrifugation. Neurobasal medium (Thermo Fisher Scientific, Landsmeer, The Netherlands) supplemented with 2 % B27 (Thermo Fisher Scientific, Landsmeer, The Netherlands), 1 % L-glutamine, and 100 U/mL penicillin-streptomycin was used to resuspend the cell pellet. Treatments were performed on day *in vitro* (DIV) 14. HT22 mouse hippocampal cells (kindly provided by Prof. Culmsee, University of Marburg, Germany), U87 MG, and U251 human glioblastoma cells (kindly provided by Prof. Frank Kruyt, University Medical Center Groningen, The Netherlands) were cultured in Dulbecco's Modified Eagle Medium (Gibco, Thermo Fisher Scientific, Landsmeer, The Netherlands) supplemented with 1 % pyruvate (only for HT22 cell culture; Thermo Fisher Scientific, Landsmeer, The Netherlands), 10 % fetal bovine serum (GE Healthcare Life Sciences, Eindhoven, the Netherlands), and 100 U/mL penicillin-streptomycin. Cultures were maintained at 37 °C and 5 % CO_2. The cells used in this study were passages between 350 and 400 and Mycoplasma free. MnTBAP, Fer (Ferrostatin-1), Lip (Liproxstatin-1), DFO (Deferoxamine), NAC (*N*-acetyl-L-cysteine), PD (PD-146176), QVD (pan-caspase inhibitor), MitoQ (Mitoquinone mesylate), and necrostatin (receptor-interacting protein kinase-1 inhibitor) were purchased from Sigma-Aldrich.

2.2. DMMB-mediated photosensitization protocol

HT22 cells, 2.10^4 cells/cm^2, were incubated with 0, 10, 25, or 50 nM DMMB (Sigma-Aldrich, Darmstadt, Germany) for 6 h at 37 °C and 5 % CO_2. Next, the medium was replaced by phosphate-buffered saline (PBS) and the cells were irradiated with a LED (BioLambda, São Paulo, BR) at 660 nm emission wavelength for 20 min, 10 J/cm^2. After irradiation, PBS was replaced by culture medium and the cells were maintained at 37 °C and 5 % CO_2 for additional 18 h. Control plates with DMMB were handled similarly and kept in the dark, instead of being irradiated.

2.3. Cytotoxicity assay

After the photosensitization protocol, cell viability was measured through 3-(4,5-dimethyl-2-thiazolyl)-2,5-diphenyl-2H-tetrazolium bromide (MTT; Sigma-Aldrich, Darmstadt, Germany) reduction assay in a 96 well plate. Cells were incubated with 0.5 mg/mL MTT for 1 h at 37 °C and 5 % CO_2. The MTT solution was then removed and 100 µL dimethyl sulfoxide (DMSO; Sigma-Aldrich, Darmstadt, Germany) was added to each well. Cells were incubated for 1 h under mild shaking at 37 °C. The absorbance of each well was determined at 570 nm with reference background absorbance at 630 nm using a Synergy H1 Multi-Mode reader (Biotek, Winooski, US). Absorption values were normalized to the average of the untreated control and converted into percentages.

2.4. Cell death measurement

After the photosensitization protocol, i.e. 18 h after irradiation, the percentage of cell death was determined by flow cytometry with the Annexin V-FITC and propidium iodide (PI) double staining kit (Thermo Fisher Scientific, Landsmeer, The Netherlands) [22]. Conditioned media and all cells were collected, stained and incubated with Annexin V-FITC and PI according to the manufacturer's instructions. Fluorescence was measured at 518 nm for FITC staining, and 617 nm for PI staining in the CytoFLEX benchtop flow cytometer (Beckman Coulter Life Sciences, Indianapolis, US). Minimum of 3 independent experiments were performed, and within an experiment 3×10^4 events were recorded for each technical replicate (at least three). Analysis was performed using FlowJo v9.0 (Becton, Dickinson and Company, Franklin Lakes, US).

2.5. Intracellular ROS measurement

After the photosensitization protocol, i.e. 18 h after irradiation, intracellular ROS was determined through staining with CM-H2DCFDA (Thermo Fisher Scientific, Landsmeer, The Netherlands). Conditioned media, washes and trypsin detached cells were collected, stained with 4 µM CM-H2DCFDA and incubated for 30 min at 37 °C. Fluorescence was excited at 492/5 nm and measured at 517/10 nm in the CytoFLEX benchtop flow cytometer (Beckman Coulter Life Sciences, Indianapolis, US). Minimum of 3 independent experiments were performed, and within an experiment 3×10^4 events were recorded for each technical replicate (at least three). Analysis was performed using FlowJo v9.0 (Becton, Dickinson and Company, Franklin Lakes, US).

2.6. Mitochondrial ROS measurement

Mitochondrial ROS after the photosensitization protocol, i.e. 18 h after irradiation, were measured by MitoSOX dye (Invitrogen, Oregon, US) staining [23]. Cells were incubated with 1.25 µM MitoSOX for 30 min at 37 °C. Next, cells were collected and fluorescence was excited at

488 nm and measured at 690/50 nm in the CytoFLEX benchtop flow cytometer (Beckman Coulter Life Sciences, Indianapolis, US). Minimum of 3 independent experiments were performed, and within an experiment 3×10^4 events were recorded for each technical replicate (at least three). Analysis was performed using FlowJo v9.0 (Becton, Dickinson and Company, Franklin Lakes, US).

2.7. Mitochondrial membrane potential measurement

After the photosensitization protocol, i.e. 18 h after irradiation, loss of mitochondrial membrane potential (ΔΨm) was measured by flow cytometry upon staining with tetramethylrhodamine-ethyl ester dye (TMRE; Invitrogen, Oregon, US) [24]. Conditioned media, washes and trypsin detached cells were collected and stained for 20 min with 0.2 μM TMRE at 37 °C. Fluorescence was measured at 690/50 nm in the CytoFLEXS benchtop flow cytometer (Beckman Coulter Life Sciences). Minimum of 3 independent experiments were performed, and within an experiment 3×10^4 events were recorded for each technical replicate (at least three). Analysis was performed using FlowJo v9.0 (Becton, Dickinson and Company).

2.8. Lipid peroxidation assessment

Lipid peroxidation after the photosensitization protocol i.e. 18 h after irradiation, was measured with the lipid peroxidation sensor BODIPY 581/591 C11 (Invitrogen, Karlsruhe, Germany). Conditioned media, washes and trypsin detached cells were collected and incubated with 2 μM staining BODIPY dye for 60 min at 37 °C. Fluorescence was excited at 500–650 nm and measured at 510–665 nm in the CytoFLEX benchtop flow cytometer (Beckman Coulter Life Sciences). Minimum of 3 independent experiments were performed, and within an experiment 3×10^4 events were recorded for each technical replicate (at least three). Analysis was performed using FlowJo v9.0 (Becton, Dickinson and Company, Indianapolis, US).

2.9. Autophagic flux assessment

Prior to the photosensitization protocol, i.e. 18 h after irradiation, HT-22 cells, at a density of 2.10^4 cells/cm^2, were transfected either with the mCherry-GFP-LC3B tandem vector or its control mCherry-GFP-LC3B G120A (pDEST-CMV mCherry-GFP-LC3B WT, Addgene plasmid # 123230; pDEST-CMV mCherry-GFP-LC3B G120A, Addgene plasmid # 123235, Addgene, Watertown, US). Both vectors were generated and made available by Robin Ketteler [25]. Transfection was performed with Attractene transfection reagent (Qiagen, Hilden, Germany) according to the manufacturer's instructions. Upon transfection with the mCherry-GFP-LC3B tandem vector, autophagosomes present both mCherry and GFP signals, while autolysosomes display only mCherry due to GFP sensibility to lower pH. For quantification, fluorescence was excited at 540–590 nm and 400–430 nm and measured at 550–650 nm and 508/520 nm for in the Guava easyCyte flow cytometer (Luminex/Diasorin, Austin, US). Minimum of 3 independent experiments were performed, and within an experiment 3×10^4 events were recorded for each technical replicate (at least three), minimum of 3 analysis was performed using FlowJo v9.0 (Becton, Dickinson and Company, Indianapolis, US).

2.10. mRNA expression profile

Autophagy related gene expression after photosensitization, i.e., 18 h after irradiation, was measured by qRT-PCR. RNA extraction was performed by organic extraction using the TRIzol reagent (ThermoFisher Scientific) according to the manufacturer's instructions. Next, 0.33 μg of total RNA was used for cDNA synthesis using the reverse transcription system (Promega, Madison, US) according to the manufacturer's instructions. All qRT-PCR reactions were performed using the FastStart Universal SYBR Green Master (Sigma-Aldrich) protocol in the Illumina Eco Real-Time PCR System (Illumina, San Diego, US). The expression of *ATG1* (forward primer: CTG TGC AAA TGG TAC AAT CAG, reverse primer: GGG CTT TGT GAT ATC TCGG), *GaBarap1* (forward primer: GGA CGC CTT ATT CTT CTT TGT C; reverse primer: TCG TGG TTG TCC TCA TAC AG), and *DRAM1* (forward primer: ATC ATC TCC TAC GTG GTC G; reverse primer TGT TCC TGT GTC ACT GGT C) were normalized by the expression of the housekeeping genes *RPL13A* (forward primer: AGA AGC AGA TCT TGA GGT TAC GG; reverse primer: GTT CAC ACC AGG AGT CCG TT) and *B2M* (forward primer: ACC GTC TAC TGG GAT CGA GA; reverse primer: TGC TAT TTC TTT CTG CGT GCA T), according to [26].

2.11. Statistical analysis

Statistical significance was evaluated using the unpaired ANOVA followed by Tukey's post-hoc test for multiple comparisons using GraphPad Prism software v.8 (GraphPad Software Inc., La Jolla, CA, USA). Data is expressed as mean ± SD. *P* values indicating statistical significance differences between mean values are represented as follows: $^*p < 0.05$, $^{**}p < 0.01$, $^{***}p < 0.001$, $^{****}p < 0.0001$.

3. Results

3.1. DMMB photosensitization mediates cell death in mouse hippocampal cell line

To address neuronal cell susceptibility to DMMB-PDT, HT22 cells were exposed to DMMB in a concentration range of 10 to 50 nM for 6 h prior to photoexcitation and the metabolic state of the cells was analyzed by an MTT assay. HT22 cells represent a well-established model to study neuronal toxicity *in vitro* [27]. After irradiation, cells were maintained in DMMB-free medium for 18 h (Fig. 1a). The evaluation of cell metabolism after the photosensitization protocol by the MTT assays revealed that activated DMMB significantly decreases the reduction of the tetrazolium salt (MTT) to formazan crystals by metabolically active HT22 cells. HT22 cell displays an IC_{50} of 22 ± 5 nM (Fig. 1a). To further evaluate the effects of DMMB on mouse primary cortical neurons, we have performed similar photosensitization experiments and observed that DMMB also reduced cellular metabolic activity (IC_{50} of 47 ± 7 nM) (Fig. 1b). This reduction is comparable to the glioblastoma cells U87 MG, IC_{50} of 26 ± 4 nM, and U251, IC_{50} of 37 ± 2 nM (Supplementary fig. 1). It is important to notice that there was no cytotoxicity upon application of the DMMB without photosensitization at any tested cells (HT22 cells, U87 MG cells, U251 cells or primary cortical neurons), when the cells were kept in the dark at room temperature (Fig. 1, Supplementary fig. 1).

To further characterize the effects of DMMB-PDT-treated cells on cell death pathways, HT22 cells were analyzed with Annexin V and PI co-staining (Fig. 2a). The Annexin V+/PI+ population was shown to be significantly increased at a concentration of 50 nM DMMB submitted to photoexcitation (termed as activated DMMB) (control: 10 ± 5 %, DMMB 50 nM: 66 ± 20 %, $n = 3$, one-way ANOVA followed by Tukey's post-hoc test, $^{**}p < 0.01$ compared to untreated control), indicating that not only the reduction of the metabolic rate, as detected by an MTT assay, but also the nuclear damage was induced by the DMMB-PDT challenge.

To further investigate the cell death pathways and whether ROS production occurs during DMMB-induced cell death in neuronal cells, we measured the formation of cellular ROS and lipid peroxidation in cells challenged with DMMB in the presence and absence of the photosensitization 18 h after irradiation. Concomitantly with the previously demonstrated cell death, there was dose-dependent increase in overall oxidative species (Fig. 2b), as detected by the oxidation of 2′,7′-dichlorodihydrofluorescein (DCFH2) to the fluorescent dichlorofluorescein (DCF) (control: 14 ± 3 %, DMMB 25 nM: 54 ± 7 %, $n = 3$, one-way ANOVA followed by Tukey's post-hoc test, $^*p < 0.05$ compared to untreated control; DMMB 50 nM: 62 ± 20 %, $n = 3$, one-way ANOVA

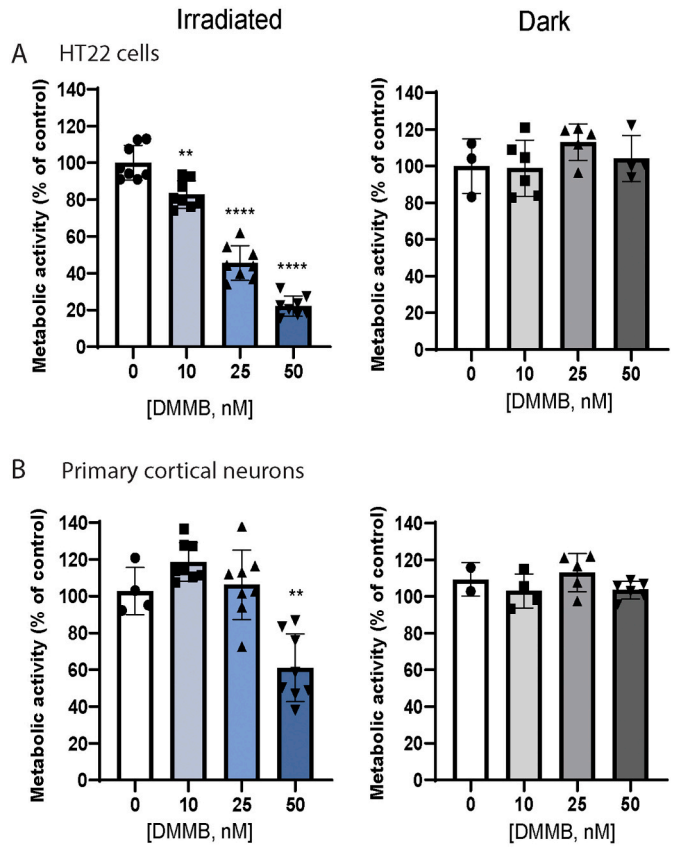

Fig. 1. DMMB photosensitization in different cell models. Cells were treated with DMMB (0, 10, 25 and 50 nM, 6 h) and irradiated with 660 nm light (10 J/cm^2), or kept in the dark, for 20 min. Cytotoxicity was evaluated by an MTT assay: (a) HT22 cells, (b) primary neurons. Data are presented as mean ± SD, n = 3–5, $^*p < 0.05$, $^{**}p < 0.01$, $^{***}p < 0.001$, $^{****}p < 0.0001$ compared to control.

followed by Tukey's post-hoc test, $^{**}p < 0.01$ compared to untreated control) (Fig. 2b). In a similar fashion, lipid peroxidation status was determined by the measurement of the oxidation of polyunsaturated butadienyl portion of BODIPY 581/591 C11, which resulted in a shift of the fluorescence emission peak from 590 to 510 nm (Fig. 2c), showing a dose-dependent increase (control: 28 ± 7; DMMB 50 nM: 68.8 ± 0.5 %, n = 3, one-way ANOVA followed by Tukey's post-hoc test, $^*p < 0.05$ compared to untreated control). Co-treatment with the superoxide dismutase (SOD) mimetic MnTBAP (Fig. 3a), which inhibits intracellular ROS generation, partially protected the cells from DMMB-PDT cytotoxicity. The pattern of protection by MnTBAP was the same regardless of the removal or not of the compound after irradiation, suggesting that MnTBAP acts upon DMMB-PDT direct ROS formation. Additionally, we employed a mitochondrially-targeted antioxidant (MitoQ) to interrogate whether targeting ROS generation in mitochondria would prevent cell death (Fig. 3g). Our results show that MitoQ had no influence on DMMB-PDT cytotoxicity. To address ferroptosis, necroptosis, or apoptosis involvement in DMMB-PDT mechanism of action, we performed the co-treatment of DMMB and various inhibitors of these processes: Ferrostatin-1 (lipid peroxidation inhibitor), Liproxstatin-1 (lipid peroxidation inhibitor) [28], Deferoxamine (non-transferrin bound iron chelator), PD-146176 (15-LOX-1 inhibitor) [29], *N*-acetyl-L-cysteine (glutathione precursor) QVD (a pan-caspase inhibitor), or necrostatin (receptor-interacting protein kinase-1 inhibitor) (Fig. 3b-f). Our data demonstrate that inhibition of ferroptosis, apoptosis, or necroptosis did not prevent DMMB-induced cell damage. Taken together, these results indicate that activated DMMB-PDT induces ROS production, which is directly implicated in its cytotoxicity, lipid peroxidation, and cell death.

3.2. DMMB photoinduced mitochondrial damage

Previous findings reported that DMMB-PDT could lead to mitochondrial damage in keratinocytes and melanoma cells [4]. Considering the importance of mitochondrial metabolism, especially for neurons and neuronal-like cells, we assessed the integrity of this organelle by investigating the function of mitochondria following DMMB-PDT challenge.

To evaluate mitochondrial status in response to activated DMMB, we focused on the mitochondrial superoxide production and mitochondrial membrane potential 18 h after irradiation. The oxidation of the fluorescent dye MitoSOX, an indicator of mitochondrial superoxide levels, was measured by flow cytometry (Fig. 4a). Exposure to activated DMMB induced a dose-dependent significant increase in mitochondrial superoxide production (control: 10 ± 4 %, DMMB 25 nM: 38 ± 9 %, $n = 3$, one-way ANOVA followed by Tukey's post-hoc test, $^{**}p < 0.01$ compared to untreated control; DMMB 50 nM: 50 ± 3 %, n = 3, one-way ANOVA followed by Tukey's post-hoc test, $^{***}p < 0.001$ compared to untreated control). Next, we measured the uptake of the cationic fluorescent dye TMRE by active mitochondria to assess mitochondrial membrane potential (ΔΨm) (Fig. 4b). DMMB photoexcitation led to a significant decrease in ΔΨm in a dose-dependent fashion (control: 28 ± 2 %, DMMB 50 nM: 51 ± 7 %, n = 3, one-way ANOVA followed by Tukey's post-hoc test, $^{**}p < 0.01$ compared to untreated control). Our data on ΔΨm are inversely correlated with the measurements of mitochondrial superoxide levels and mitochondrial fragmentation in the presence of DMMB-induced PDT and neuronal cell death, suggesting increased ROS production as a result of damaged mitochondria.

3.3. DMMB photoinduced autophagy flux impairment

We have previously demonstrated that activated DMMB impairs autophagy in keratinocytes and melanoma cells [4]. LC3 (microtubule-associated protein 1 (MAP1) light chain 3) is a classical autophagy marker that after post-translational processing is incorporated into autophagosomes. To investigate the effect of DMMB-PDT in the autophagic flux in neuronal cells, we made use of the tandem-tagged mCherry-EGFP-LC3B [25], which indirectly reports LC3 subcellular localization by measuring degradation of EGFP by acidic lysosomal environment upon autophagolysosome formation (Fig. 5a). Exposure to activated DMMB induced a significant increase of acidic autophagolysosomes, indicating the DMMB may increase autophagic flux in neuronal cells (control: 19 ± 2 %, DMMB 25 nM: 26 ± 2 %, $n = 3$, one-way ANOVA followed by Tukey's post-hoc test, $^{**}p < 0.01$ compared to untreated control±; DMMB 50 nM: 26 ± 0.5 %, n = 3, one-way ANOVA followed by Tukey's post-hoc test, $^{**}p < 0.01$ compared to untreated control) (Fig. 5b). This increase in the number of acidic autophalolysosomes is accompanied by an increase in the colocalization of mitochondria and lysossomes (Supplementary fig. 2). Noteworthy, the inhibition of the ULK-complex, involved in autophagosome formation, partially protects the cells against DMMB-PDT induced cell death (Supplementary fig. 3b). While the inhibition of lysosomal fusion to autophagosomes does not affect cell death at all (Supplementary fig. 3a). In line with previous research from our group [4], our results suggest that the damage is parallelly inflicted in mitochondrial and lysosomal membranes.

To evaluate key steps during autophagy, such as phagophore assembly, mitochondrial commitment to mitophagy, and lysosomal acidification, we analyzed gene expression of Autophagy Related 1 (*ATG1*), GaBarap1 (*GABA Type A Receptor-Associated Protein*), and Damage-regulated autophagy modulator 1 (*DRAM1*) – autophagy related genes, respectively. Our data showed that 50 nM activated DMMB significantly upregulated *ATG1* (control: 1 ± 0.1; DMMB 50 nM: 1.8 ± 0.5, $n \geq 3$, one-way ANOVA followed by Tukey's post-hoc test, $^{***}p < 0.001$ compared to untreated control) (Fig. 4c). In addition, *ATG8* homologue *GaBarap1* expression was also significantly upregulated upon

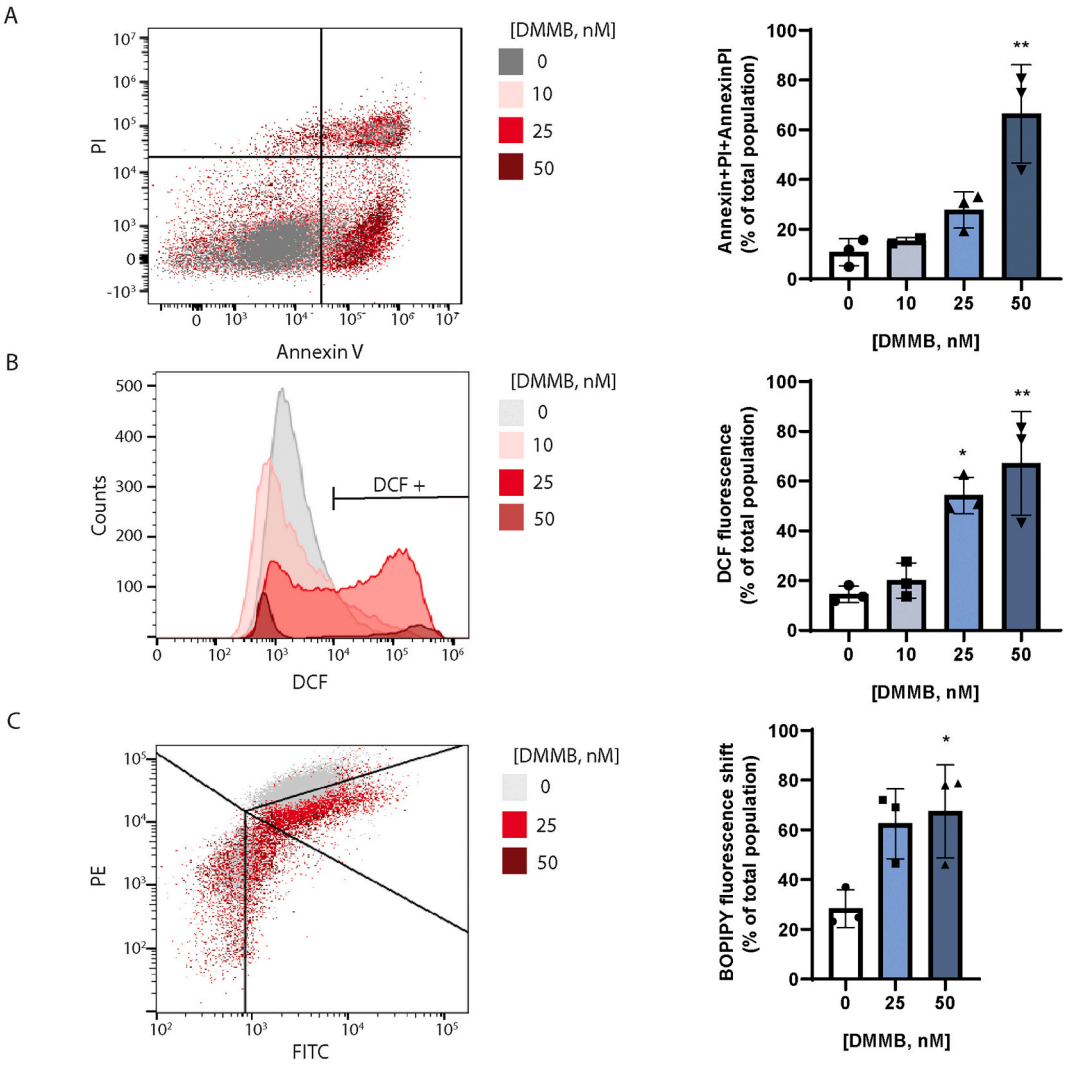

Fig. 2. DMMB mediated photoinduced cell death and ROS generation. HT22 cells treated with DMMB (10, 25 and 50 nM, 6 h) and irradiated with 660 nm light (10 J/cm^2) for 20 min. Cell death was evaluated through (a) Annexin V/PI staining by flow cytometry. (b) Overall cellular ROS were measured by DCF staining and (c) lipid peroxidation by BODIPY staining. Data are presented as mean ± SD, n = 3–5, $*p < 0.05$, $**p < 0.01$, compared to control.

activated DMMB exposure (control: 1 ± 0.2; DMMB 25 nM: 2.9 ± 0.8, n ≥ 3, one-way ANOVA followed by Tukey's post-hoc test, $**p < 0.01$ compared to untreated control; DMMB 50 nM: 2.8 ± 0.3, n ≥ 3, one-way ANOVA followed by Tukey's post-hoc test, $**p < 0.01$ compared to untreated control) (Fig. 4d). On the other hand, the highest concentration of activated DMMB tested led to a significant decrease in *DRAM1* expression (control: 1.05 ± 0.06, DMMB 50 nM: not detected, n ≥ 3, one-way ANOVA followed by Tukey's post-hoc test, $***p < 0.001$ compared to untreated control) (Fig. 4e). Both *ATG1* and *GaBarap1* increased expression in response to activated DMMB challenge indicate that DMMB-PDT is able to induce autophagy in neuronal cells. While decrease in *DRAM1* indicates a dysfunction in late stages of autophagosome clearance, which could lead to the accumulation of acidic autophagolysosomes. Next, we investigated the dependence of DMMB-PDT mediated cell death on ATG7, involved in mitophagy, and ATG13, involved in mTor dependent autophagosome formation (Supplementary Fig. 4). We observed that ATG7 siRNA is protective against DMMB-PDT, while ATG13 is not. These data indicate that DMMB-PDT might initiate neuronal cell death via mitochondrial dysfunction and an increased autophagy flux in conjunction with impairment in the late stages of autophagy.

4. Discussion

PDT-directed cytotoxicity has been shown to be a promising tool for the treatment of conditions such as brain tumors [8,9]. The effect of PDT on healthy neurons is one main concern over its use in the CNS, since neuronal cells could be particularly sensitive to certain PSs [11]. This study provides insights into the effects of DMMB-PDT on neuronal-like HT22 cells.

Previous studies have proposed that the efficiency of anti-cancer approaches, including PDT is higher in tumor cells with an increased autophagic index [30–35]. In a similar manner, several mitochondrial-targeting therapies have shown promising results in cancer, aging and neurodegeneration [36–38]. For instance, increasing mitochondrial fitness and mitochondrial resilience to stress with mitochondrial complex I inhibitors was shown to decrease glioma aggressiveness *in vitro* and improve overall survival of patients with grade III gliomas [39–41], as well as increasing neurogenesis and improved cognitive function [42]. Nevertheless, the addition of a mitochondria-targeting moiety to PSs has been proposed as a strategy to increase their potency by concentrating ROS production to this organelle and therefore increase cytotoxicity [43].

The phenothiazinium chromophore DMMB is a highly efficient PS

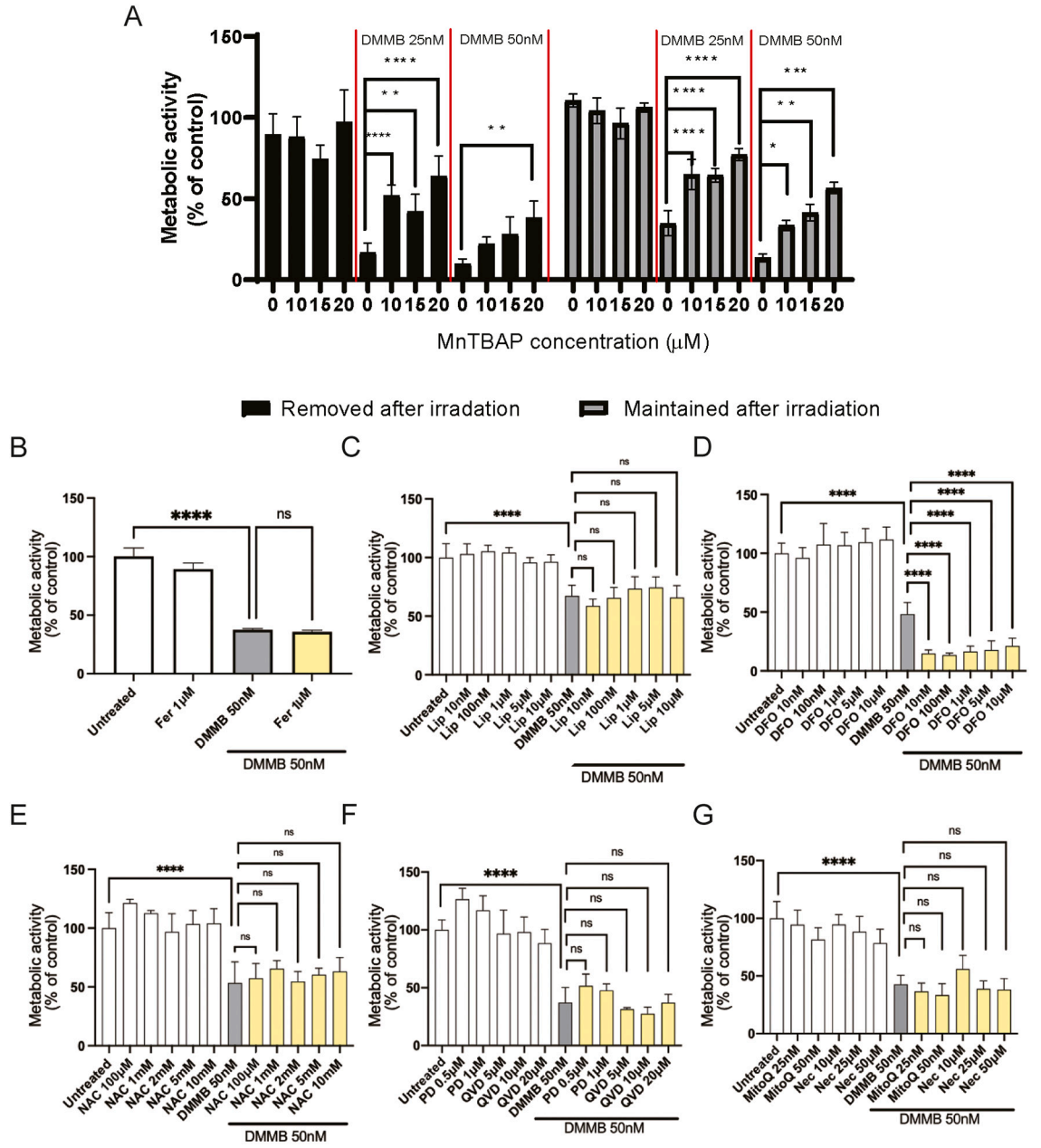

Fig. 3. Effects of inhibitors of ferroptosis, apoptosis, necroptosis or mitochondrial ROS generation on DMMB-induced cell death. HT22 cells were treated with DMMB (50 nM, 6 h), and co-treated with different pharmacological modulators of cell death pathways. After 6 h, cells were irradiated with 660 nm light (11 J/cm^2) for 20 min. (a) MnTBAP, (b) Fer (Ferrostatin-1), (c) Lip (Liproxstatin-1), (d) DFO (Deferoxamine), (e) NAC (*N*-acetyl-L-cysteine), (f) PD (PD-146176), QVD (pan-caspase inhibitor); and (g) MitoQ (Mitoquinone mesylate), Nec (necrostatin). Representative plots from 3 independent experiments. Data are presented as mean ± SD, $n = 8$ ***$p < 0.001$; ****$p < 0.001$.

with an absorbance peak of 651 nm [30]. In fact, DMMB has been shown to more efficiently produce singlet-oxygen and have lower IC_{50} in melanoma cells when compared to its counterpart MB [4,20]. We have previously described that these positively charged dyes accumulate in both mitochondria and lysosomes [4]. Additionally, DMMB is more resistant to reduction than MB and it was shown to localize in mitochondria of mammalian cells, inducing selective mitochondrial DNA damage [4,45]. Co-treatment with the superoxide dismutase (SOD) mimetic MnTBAP partially protected the cells from DMMB-PDT cytotoxicity. This effect was not seen with the co-treatment with the mitochondrially-targeted antioxidant MitoQ, which suggests that direct DMMB-PDT intracellular ROS generation mediates organelle damage and induces cell death. MB-PDT was shown to induce necroptosis [46], remarkably the same is not observed here. In fact, the co-treatment of DMMB with necroptosis, ferroptosis or apoptosis inhibitors failed to protect the cells against DMMB-PDT cytotoxicity.

Our results demonstrate that DMMB-PDT-associated decrease in cell viability was linked to an increase in cellular ROS production and lipid peroxidation. These ROS measurements detect both DMMB-PDT and ROS produced by mitochondria. Moreover, DMMB-PDT treatment resulted in a significant increase in mitochondrial superoxide production and decrease in ΔΨm. Our results indicate that DMMB-PDT could mediate cell death by affecting mitochondrial function.

Previous data from our group showed that in keratinocytes DMMB-PDT impairs autophagy more effectively than MB-PDT [4]. To assess whether autophagy impairment is also taking place in neurons we used the tandem-tagged mCherry-EGFP-LC3B system. LC3 (microtubule-associated protein 1 (MAP1) light chain 3) is a classical autophagy

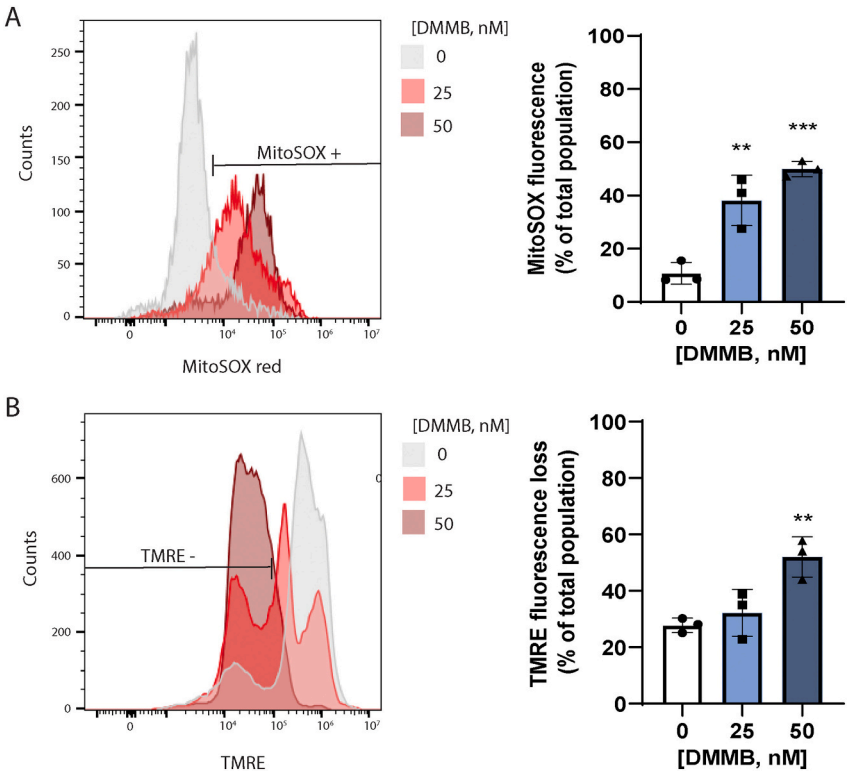

Fig. 4. DMMB mediated photoinduced mitochondrial alterations. HT22 cells treated with DMMB (25 and 50 nM, 6 h) irradiated with 660 nm light (10 J/cm^2) for 20 min. Mitochondrial superoxide levels using (a) MitoSOX and (b) ΔΨm loss using TMRE were determined by flow cytometry. Data are presented as mean ± SD, $n = 3$, $^{**}p < 0.01$, $^{***}p < 0.001$ compared to control.

marker that after post-translational processing is incorporated into autophagosomes. This system makes use of EGFP higher susceptibility to pH when compared to mCherry to monitor autophagy status. The pH drops to around 4.8 [45] in response to autophagosomes fusion to lysosomes that forms autolysosomes and leads to the degradation of EGFP, while mCherry remains stable. Our results showed a significant increase in the presence of acidic autophagolysosomes accompanied by an increase in damaged mitochondria and lysosome colocalization, suggesting their accumulation in response to DMMB-PDT. Furthermore, blocking autophagosome formation through the inhibition of the ULK-complex [47-49], partially protects the cells against DMMB-PDT induced cell death. To further evaluate autophagy involvement in DMMB-PDT, we downregulated *ATG7* prior to DMMB-PDT. ATG7 is a central player for autophagy induction by acting like an E1 enzyme for ubiquitin-like proteins such as ATG12 and ATG8, making it a crucial regulator of autophagosome assembly [47]. We observed that DMMB-PDT-cell death is dependent on ATG7, with its downregulation being partially protecting. Additionally, ATG7 deficiencies are implicated in mitochondrial quality control defects [49], further supporting the role of mitophagy in DMMB-PDT-cell death. Our results suggest that inhibition of autophagosome assembly might extenuate the downstream lysosomal-dysfunction that triggers cell death.

To better characterize the mechanism taking place, we analyzed the expression of the phagosome formation and maturation markers *ATG1* and the ATG8 homologue *GaBarap1* [50–53]. *ATG1* expression is an early marker of autophagy activation, as it is involved in the organization of the initial phagophore at the phagophore assembly site [50]. In turn, *GaBarap1* plays a key role during formation and maturation of the autophagosome. ATG8 proteins conjugate to specific adaptors during selective autophagy, such as mitophagy, and guide the vesicles containing the cargo through microtubules to the autophagosomes [51]. The increased expression of these genes suggests that autophagy is promoted by DMMB-PDT.

To further explore the autophagic flux triggered by DMMB, *DRAM1* expression was determined. DRAM1 protein is a key player in the clearance of autophagosomes by promoting lysosome acidification and activation of lysosomal enzymes, being involved in autophagosome clearance [53]. Moreover, *DRAM1* expression is induced by p53 and increases apoptosis by preventing BAX degradation [54,55]. Here, we observed a significant decrease in the expression of *DRAM1* by DMMB-PDT in HT22 cells, which suggests an autophagy dysfunction in late stages of the process.

Our results are in agreement with our previous report which demonstrates that DMMB-PDT autophagy-related cell death in Hek293T cells is independent of p53 status [44]. This is particularly relevant for CNS tumors, since the p53-ARF-MDM2 pathway is found deregulated in 84 % of GBM patients [56]. Nevertheless, *DRAM1* knockdown in mycobacteria-infected macrophages was shown to lead to premature cell death in a mechanism dependent on Caspase a (Caspa) and Gasdermin eb (Gsmdeb), which suggests pyroptosis is responsible for the cell demise [57]. Autophagy impairment has been correlated with pyroptosis activation in different models [57–61], suggesting that the autophagy-pyroptosis crosstalk might be involved in DMMB-PDT cell death. Taken together our results indicate that DMMB-PDT acts by damaging mitochondria and by possibly impairing autophagy.

CRediT authorship contribution statement

RANG, MSB, AMD, and MTL: conceptualization, original draft preparation, data analysis, manuscript revision. **RANG, AMG, FJH, TMG, TC, YMFP and MMM**: performed experiments, data analysis. **SKNM, MM and MSB**: data analysis, manuscript revision.

Declaration of competing interest

The authors declare that they have no known competing financial

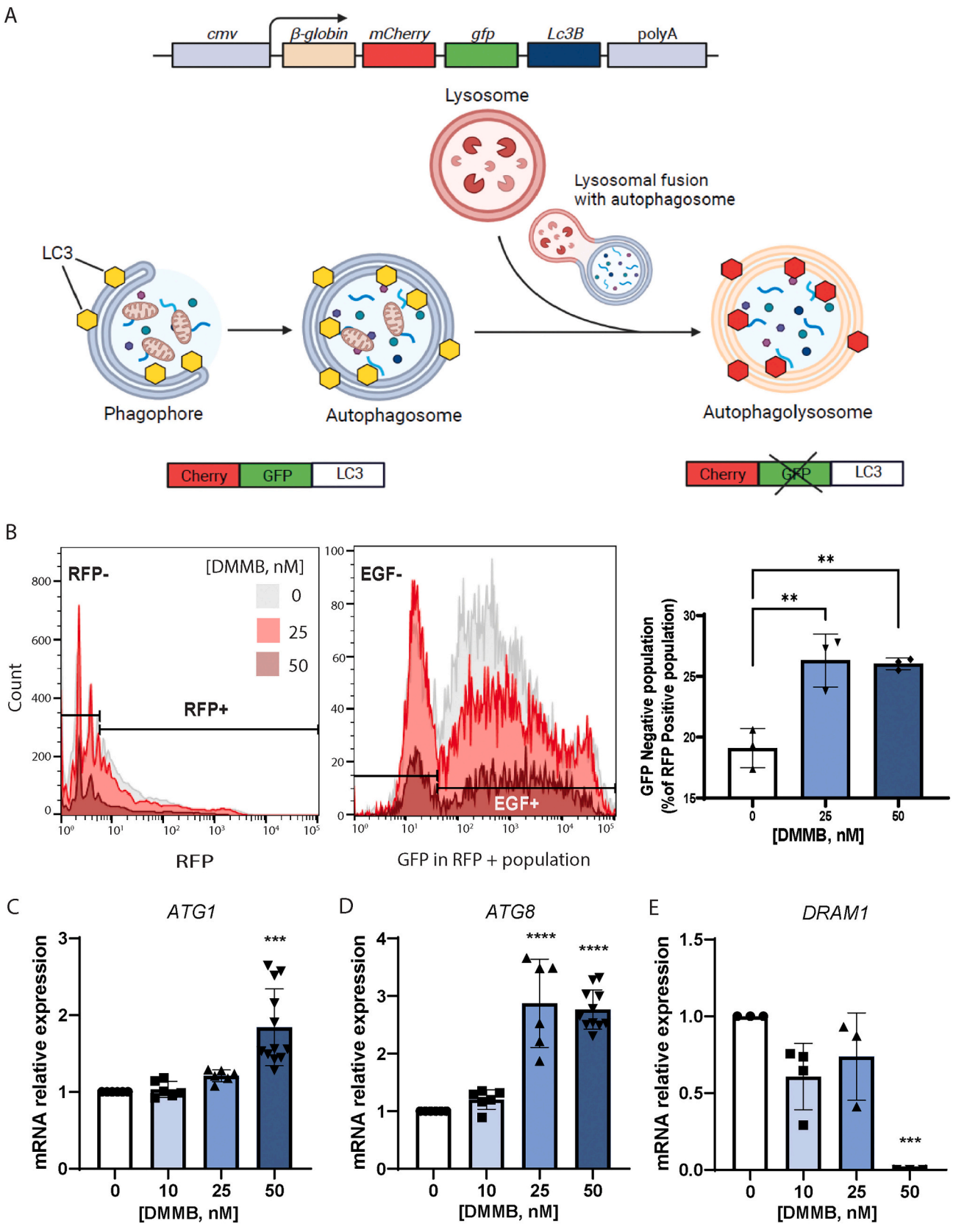

Fig. 5. DMMB mediated autophagy dysfunction. HT22 cells treated with DMMB (10, 25 and 50 nM, 6 h) kept in the dark or irradiated with 660 nm light (10 J/cm^2) for 20 min. (a) Cells were transfected with the tandem-tagged mCherry-EGFP-LC3B or its mutated control mCherry-EGFP-LC3B G120A prior to DMMB treatment. The drawing was created using BioRender.com. GFP fluorescence is quenched in the acidic environment of the autolysosomes, whereas the red fluorescence is preserved, allowing (b) monitoring of the autophagic flux by flow cytometry. Relative mRNA expression of the autophagy-related genes (b) *Atg1*, (c) *GaBarap1* (*ATG8 homologue*), and (d) *Dram1*. Data are presented as mean ± SD, n = 3–5, *$p < 0.05$, **$p < 0.01$, ***$p < 0.001$, ****$p < 0.0001$, compared to control.

interests or personal relationships that could have appeared to influence the work reported in this paper.

Data availability

Data will be made available on request.

Acknowledgements

A.M.D. is the recipient of a Rosalind Franklin Fellowship co-funded by the European Union and the University of Groningen. M.T.L. was the recipient of a CAPES Fellowship (process# 88887.321693/2019-00). A.M.G. is financially supported by the GSMS (Graduate School of Medical Sciences, UMCG/RUG, Groningen, The Netherlands) and CONACYT (Mexico). T.C. is financially supported by China Scholarship Council (China) (grant # 202006990022). Y.E.M.F.P. was the recipient of a CNPq Fellowship (process# 140106/2019-7). S.K.N.M. acknowledges CAPES (Brazil), NUFFIC (The Netherlands) (grant no 062/15, process #9999.001625/2015-02). MSB acknowledges FAPESP CEPID-Redoxoma (Brazil) (grant # 2013/07937-8) and CNPq (Brazil) (grant # 303831/2019-7).

Appendix A. Supplementary data

Supplementary data to this article can be found online at https://doi.org/10.1016/j.bbamcr.2022.119429.

References

[1] R.R. Allison, K. Moghissi, Photodynamic therapy (PDT): PDT mechanisms, Clin Endosc. 46 (1) (2013) 24–29.
[2] L. Benov, Photodynamic therapy: current status and future directions, Med. Princ. Pract. 24 (Suppl 1) (2015) 14–28.
[3] D. Kessel, Subcellular targets for photodynamic therapy: implications for initiation of apoptosis and autophagy, J. Natl. Compr. Cancer Netw. 10 (Suppl 2) (2012) S56–S59.
[4] W.K. Martins, N.F. Santos, C.S. Rocha, I.O.L. Bacellar, T.M. Tsubone, A.C. Viotto, et al., Parallel damage in mitochondria and lysosomes is an efficient way to photoinduce cell death, Autophagy 15 (2) (2019) 259–279.
[5] K. Plaetzer, M. Berneburg, T. Kiesslich, T. Maisch, New applications of photodynamic therapy in biomedicine and biotechnology, Biomed. Res. Int. 2013 (2013), 161362.
[6] S.L. Marcus, W.R. McIntyre, Photodynamic therapy systems and applications, Expert Opin. Emerg. Drugs 7 (2) (2002) 321–334.
[7] A.B. Uzdensky, O.Y. Dergacheva, A.A. Zhavoronkova, A.V. Ivanov, A. V. Reshetnikov, G.V. Ponomarev, Photodynamic effect of deuteroporphyrin IX and hematoporphyrin derivatives on single neuron, Biochem. Biophys. Res. Commun. 281 (5) (2001) 1194–1199.
[8] M.A. Rosenthal, B. Kavar, S. Uren, A.H. Kaye, Promising survival in patients with high-grade gliomas following therapy with a novel boronated porphyrin, J. Clin. Neurosci. 10 (4) (2003) 425–427.
[9] H. Hirschberg, D.R. Sørensen, E. Angell-Petersen, Q. Peng, B. Tromberg, C.H. Sun, et al., Repetitive photodynamic therapy of malignant brain tumors, J. Environ. Pathol. Toxicol. Oncol. 25 (1–2) (2006) 261–279.
[10] M.W. Leach, S. Khoshyomn, J. Bringus, S.A. Autry, J.E. Boggan, Normal brain tissue response to photodynamic therapy using aluminum phthalocyanine tetrasulfonate in the rat, Photochem. Photobiol. 57 (5) (1993) 842–845.
[11] Q. Chen, M. Chopp, L. Madigan, M.O. Dereski, F.W. Hetzel, Damage threshold of normal rat brain in photodynamic therapy, Photochem. Photobiol. 64 (1) (1996) 163–167.
[12] K.E. Wright, A.J. MacRobert, J.B. Phillips, Inhibition of specific cellular antioxidant pathways increases the sensitivity of neurons to meta-tetrahydroxyphenyl chlorin-mediated photodynamic therapy in a 3D co-culture model, Photochem. Photobiol. 88 (6) (2012) 1539–1545.
[13] A. Miclescu, H.S. Sharma, C. Martijn, L. Wiklund, Methylene blue protects the cortical blood-brain barrier against ischemia/reperfusion-induced disruptions, Crit. Care Med. 38 (11) (2010) 2199–2206.
[14] J. Shen, W. Xin, Q. Li, Y. Gao, L. Yuan, J. Zhang, Methylene blue reduces neuronal apoptosis and improves blood-brain barrier integrity after traumatic brain injury, Front. Neurol. 10 (2019) 1133.
[15] Y. Wen, W. Li, E.C. Poteet, L. Xie, C. Tan, L.J. Yan, et al., Alternative mitochondrial electron transfer as a novel strategy for neuroprotection, J. Biol. Chem. 286 (18) (2011) 16504–16515.
[16] E. Poteet, G.R. Choudhury, A. Winters, W. Li, M.G. Ryou, R. Liu, et al., Reversing the Warburg effect as a treatment for glioblastoma, J. Biol. Chem. 288 (13) (2013) 9153–9164.
[17] C. Peter, D. Hongwan, A. Küpfer, B.H. Lauterburg, Pharmacokinetics and organ distribution of intravenous and oral methylene blue, Eur. J. Clin. Pharmacol. 56 (3) (2000) 247–250.
[18] D.A. Santos, P.J.L. Crugeira, I.P.F. Nunes, P.F. de Almeida, A.L.B. Pinheiro, A novel technique of antimicrobial photodynamic therapy - aPDT using 1,9-dimethyl-methylene blue zinc chloride double salt-DMMB and polarized light on Staphylococcus aureus, J. Photochem. Photobiol. B 200 (2019), 111646.
[19] B.I. Lee, Y.S. Suh, Y.J. Chung, K. Yu, C.B. Park, Shedding light on Alzheimer's β-amyloidosis: photosensitized methylene blue inhibits self-assembly of β-amyloid peptides and disintegrates their aggregates, Sci. Rep. 7 (1) (2017) 7523.
[20] M. Wainwright, D.A. Phoenix, L. Rice, S.M. Burrow, J. Waring, Increased cytotoxicity and phototoxicity in the methylene blue series via chromophore methylation, J. Photochem. Photobiol. B 40 (3) (1997) 233–239.
[21] V. Rangaraju, T.L. Lewis, Y. Hirabayashi, M. Bergami, E. Motori, R. Cartoni, et al., Pleiotropic mitochondria: the influence of mitochondria on neuronal development and disease, J. Neurosci. 39 (42) (2019) 8200–8208.
[22] M. Trombetta-Lima, I.E. Krabbendam, A.M. Dolga, Calcium-activated potassium channels: implications for aging and age-related neurodegeneration, Int. J. Biochem. Cell Biol. 123 (2020), 105748.
[23] B. Honrath, L. Matschke, T. Meyer, L. Magerhans, F. Perocchi, G.K. Ganjam, et al., SK2 channels regulate mitochondrial respiration and mitochondrial ca, Cell Death Differ. 24 (5) (2017) 761–773.
[24] M. Richter, C. Nickel, L. Apel, A. Kaas, R. Dodel, C. Culmsee, et al., SK channel activation modulates mitochondrial respiration and attenuates neuronal HT-22 cell damage induced by H2O2, Neurochem. Int. 81 (2015) 63–75.
[25] A. Agrotis, N. Pengo, J.J. Burden, R. Ketteler, Redundancy of human ATG4 protease isoforms in autophagy and LC3/GABARAP processing revealed in cells, Autophagy 15 (6) (2019) 976–997.
[26] M.W. Pfaffl, A new mathematical model for relative quantification in real-time RT-PCR, Nucleic Acids Res. 29 (9) (2001), e45.
[27] S. Neitemeier, A. Jelinek, V. Laino, L. Hoffmann, I. Eisenbach, R. Eying, et al., BID links ferroptosis to mitochondrial cell death pathways, Redox Biol. 12 (2017) 558–570.
[28] G. Miotto, M. Rossetto, M.L. Di Paolo, L. Orian, R. Venerando, A. Roveri, A. M. Vučković, V. Bosello Travain, M. Zaccarin, L. Zennaro, M. Maiorino, S. Toppo, F. Ursini, G. Cozza, Insight into the mechanism of ferroptosis inhibition by ferrostatin-1, Redox Biol. 28 (2020), 101328.
[29] O. Zilka, R. Shah, B. Li, J.P. Friedmann Angeli, M. Griesser, M. Conrad, D.A. Pratt, On the mechanism of cytoprotection by Ferrostatin-1 and Liproxstatin-1 and the role of lipid peroxidation in ferroptotic cell death, ACS Cent Sci. 3 (3) (2017) 232–243.
[30] I.O. Bacellar, C. Pavani, E.M. Sales, R. Itri, M. Wainwright, M.S. Baptista, Membrane damage efficiency of phenothiazinium photosensitizers, Photochem. Photobiol. 90 (4) (2014) 801–813.
[31] X.H. Ma, S. Piao, D. Wang, Q.W. McAfee, K.L. Nathanson, J.J. Lum, et al., Measurements of tumor cell autophagy predict invasiveness, resistance to chemotherapy, and survival in melanoma, Clin. Cancer Res. 17 (10) (2011) 3478–3489.
[32] J. Klose, M.V. Stankov, M. Kleine, W. Ramackers, D. Panayotova-Dimitrova, M. D. Jäger, et al., Inhibition of autophagic flux by salinomycin results in anti-cancer effect in hepatocellular carcinoma cells, PLoS One 9 (5) (2014), e95970.
[33] H. Du, W. Yang, L. Chen, M. Shi, V. Seewoo, J. Wang, et al., Role of autophagy in resistance to oxaliplatin in hepatocellular carcinoma cells, Oncol. Rep. 27 (1) (2012) 143–150.
[34] B. Zhai, F. Hu, X. Jiang, J. Xu, D. Zhao, B. Liu, et al., Inhibition of akt reverses the acquired resistance to sorafenib by switching protective autophagy to autophagic cell death in hepatocellular carcinoma, Mol. Cancer Ther. 13 (6) (2014) 1589–1598.
[35] N. Xu, J. Zhang, C. Shen, Y. Luo, L. Xia, F. Xue, et al., Cisplatin-induced downregulation of miR-199a-5p increases drug resistance by activating autophagy in HCC cell, Biochem. Biophys. Res. Commun. 423 (4) (2012) 826–831.
[36] S. Stolik, J.A. Delgado, A. Pérez, L. Anasagasti, Measurement of the penetration depths of red and near infrared light in human "ex vivo" tissues, J. Photochem. Photobiol. B 57 (2–3) (2000) 90–93.
[37] M. Trombetta-Lima, A.M. Sabogal-Guáqueta, A.M. Dolga, Mitochondrial dysfunction in neurodegenerative diseases: a focus on iPSC-derived neuronal models, Cell Calcium 94 (2021), 102362.
[38] S.E. Weinberg, N.S. Chandel, Targeting mitochondria metabolism for cancer therapy, Nat. Chem. Biol. 11 (1) (2015) 9–15.
[39] P.H. Reddy, Mitochondrial medicine for aging and neurodegenerative diseases, Neuromolecular Med. 10 (4) (2008) 291–315.
[40] R. Würth, A. Pattarozzi, M. Gatti, A. Bajetto, A. Corsaro, A. Parodi, et al., Metformin selectively affects human glioblastoma tumor-initiating cell viability: a role for metformin-induced inhibition of akt, Cell Cycle 12 (1) (2013) 145–156.
[41] M. Mazurek, J. Litak, P. Kamieniak, B. Kulesza, K. Jonak, J. Baj, et al., Metformin as potential therapy for high-grade glioma, Cancers (Basel) 12 (1) (2020).
[42] C. Seliger, C. Luber, M. Gerken, J. Schaertl, M. Proescholdt, M.J. Riemenschneider, et al., Use of metformin and survival of patients with high-grade glioma, Int. J. Cancer 144 (2) (2019) 273–280.
[43] S. Ahmed, Z. Mahmood, A. Javed, S.N. Hashmi, I. Zerr, S. Zafar, et al., Effect of metformin on adult hippocampal neurogenesis: comparison with donepezil and links to cognition, J. Mol. Neurosci. 62 (1) (2017) 88–98.
[44] S.M. Mahalingam, J.D. Ordaz, P.S. Low, Targeting of a photosensitizer to the mitochondrion enhances the potency of photodynamic therapy, ACS Omega. 3 (6) (2018) 6066–6074.

[45] A.B.P. Abrantes, G.C. Dias, N.C. Souza-Pinto, M.S. Baptista, p53-dependent and p53-independent responses of cells challenged by photosensitization, Photochem. Photobiol. 95 (1) (2019) 355–363.
[46] D.R.Q. de Almeida, A.F. Dos Santos, R.A.M. Wailemann, L.F. Terra, V.M. Gomes, G. S. Arini, E.R.M. Bertoldi, E.M. Reis, M.S. Baptista, L. Labriola, Necroptosis activation is associated with greater methylene blue-photodynamic therapy-induced cytotoxicity in human pancreatic ductal adenocarcinoma cells, Photochem Photobiol Sci. (2022), https://doi.org/10.1007/s43630-022-00347-4.
[47] D.J. Klionsky, B.A. Schulman, Dynamic regulation of macroautophagy by distinctive ubiquitin-like proteins, Nat. Struct. Mol. Biol. 21 (4) (2014) 336–345.
[48] C.H. Jung, C.B. Jun, S.H. Ro, et al., ULK-Atg13-FIP200 complexes mediate mTOR signaling to the autophagy machinery, Mol. Biol. Cell 20 (7) (2009) 1992–2003.
[49] H. Nahapetyan, M. Moulis, E. Grousset, et al., Altered mitochondrial quality control in Atg7-deficient VSMCs promotes enhanced apoptosis and is linked to unstable atherosclerotic plaque phenotype, Cell Death Dis. 10 (2019) 119.
[50] S. Ohkuma, B. Poole, Fluorescence probe measurement of the intralysosomal pH in living cells and the perturbation of pH by various agents, Proc. Natl. Acad. Sci. U. S. A. 75 (7) (1978) 3327–3331.
[51] G. Stjepanovic, C.W. Davies, R.E. Stanley, M.J. Ragusa, D.J. Kim, J.H. Hurley, Assembly and dynamics of the autophagy-initiating Atg1 complex, Proc. Natl. Acad. Sci. U. S. A. 111 (35) (2014) 12793–12798.
[52] Y.K. Lee, J.A. Lee, Role of the mammalian ATG8/LC3 family in autophagy: differential and compensatory roles in the spatiotemporal regulation of autophagy, BMB Rep. 49 (8) (2016) 424–430.
[53] F.Z. Chakrama, S. Seguin-Py, J.N. Le Grand, A. Fraichard, R. Delage-Mourroux, G. Despouy, V. Perez, M. Jouvenot, M. Boyer-Guittaut, GABARAPL1 (GEC1) associates with autophagic vesicles, Autophagy 6 (4) (2010) 495–505.
[54] T. Shpilka, H. Weidberg, S. Pietrokovski, Z. Elazar, Atg8: an autophagy-related ubiquitin-like protein family, Genome Biol. 12 (7) (2011) 226.
[55] X.D. Zhang, L. Qi, J.C. Wu, Z.H. Qin, DRAM1 regulates autophagy flux through lysosomes, PLoS One 8 (5) (2013), e63245.
[56] D. Crighton, S. Wilkinson, K.M. Ryan, DRAM links autophagy to p53 and programmed cell death, Autophagy 3 (1) (2007) 72–74.
[57] R. Zhang, M. Varela, G. Forn-Cuní, V. Torraca, M. van der Vaart, A.H. Meijer, Deficiency in the autophagy modulator Dram1 exacerbates pyroptotic cell death of mycobacteria-infected macrophages, Cell Death Dis. 11 (4) (2020) 277.
[58] Y. Zhang, C. Dube, M. Gibert, N. Cruickshanks, B. Wang, M. Coughlan, et al., The p53 pathway in glioblastoma, Cancers (Basel) 10 (9) (2018).
[59] T. Zheng, C. Zhao, B. Zhao, H. Liu, S. Wang, L. Wang, et al., Impairment of the autophagy-lysosomal pathway and activation of pyroptosis in macular corneal dystrophy, Cell Death Discov. 6 (1) (2020) 85.
[60] C. Chung, W. Seo, P. Silwal, E.K. Jo, Crosstalks between inflammasome and autophagy in cancer, J. Hematol. Oncol. 13 (1) (2020) 100.
[61] R. Guo, H. Wang, N. Cui, Autophagy regulation on pyroptosis: mechanism and medical implication in sepsis, Mediat. Inflamm. 2021 (2021) 9925059.